CHANGING PATTERN OF THE SHORELINE GEOMETRY AS OBSERVED IN CHITTAGONG DISTRICT

Reaz A Mullick*[1] and Ashraful Islam[2]

[1] Professor, Chittagong University of Engineering and Technology (CUET), Bangladesh, e-mail: reazmullick@cuet.ac.bd
[2] Research Assistant, Chittagong University of Engineering and Technology (CUET), Bangladesh, e-mail: ashraful.cuetbd@gmail.com

ABSTRACT

In this research, the dynamicity of the shoreline geometry of Chittagong district of Bangladesh is unveiled in terms of temporal and spatial change. The shoreline is divided into three segments according to their three different spatial distributions. Multi temporal LANDSAT images were used to monitor shoreline positional change from the year 1977 to 2017. LANDSAT images were radiometrically corrected and McFeeters' normalized difference water index (NDWI) was calculated to effectively differentiate water and land features. A histogram based thresholding method along with scene based visual interpretation was used to extract the shorelines. Linear Regression Rate (LRR) was calculated for determining shoreline rate-of-change . Analysis based on the images of last 40 years shows that, the shoreline is shifting towards landward in the entire study area with different rates. In the northern segment, the average rate is 2.56 m/yr. More than 3.36 km^2 land area was withdrawn and 1.76 km^2 land area was gained. In the middle segment, the rate of shoreline shifting is 6.01 m/yr and more than 2.9 km^2 area was lost. No significant land area is gained. In the southern segment, the average shifting rate of 4.37 m/yr is seen landwards and more than 6.4 km^2 area was lost. Little over 0.17 km^2 land area was gained. Overall, for the last 40 years, a 12.66 km^2 land area withdrawn and 1.93 km^2 land area loss are observed along the shoreline of Chittagong district.

Keywords: *Shoreline Change Rate, Chittagong, Remote Sensing, Weighted Linear Regression*

1. INTRODUCTION

Shoreline is a line that coincides with the physical interface of land and sea or other water feature (Dolan et al., 1980). While conducting any analysis on the shoreline or its geometry, it must be considered in a temporal sense, and the time scale chosen will depend on the context of the investigation (Boak and Turner, 2005). In their paper, Boak and Turner also commented that Remote Sensing (RS) is becoming popular now-a-days to detect shoreline using multispectral and hyper-spectral satellite imaging and being widely used globally by many scientists and researchers which is evident in the works of Li and Damen, 2010, Alesheikh, Ghorbanali and Nouri, 2007, Bouchahma and Yan, 2012, Kuleli, et al., 2011, Siripong, 2010 etc. RS along with Geographic Information System (GIS) technologies are used to determine the dynamic nature of shore as well as to detect and monitor temporal and spatial change of an existing water feature (Erener and Yakar, 2012). RS and GIS were also used by Mukhopadhyay et al., 2012 to detect and analyze shoreline where they used multi temporal LANDSAT images from United States Geological Survey (USGS) agency. In this study, remotely sensed satellite LANDSAT images were used to detect shoreline position of Chittagong coastal zone of Bangladesh in different years. These orthorectified and radiometrically corrected images are used in this study furthermore to determine the shoreline geometry and their change rate in a temporal basis. It is noted that a shoreline of a coastal zone has a dynamic environment where shoreline can change due to various factors such as coastal erosion and deposition, tides, storms, biological activities and man-made causes (Kostiuk, 2002).

The shoreline of Bangladesh is of dynamic in nature. As there is a lack of steadiness, the conception that a rising sea-level with global warming will submerge Bangladesh's coastal area is somewhat an exaggerated statement (Brammer, 2013). A systematic assessment of rates of shoreline change of Bangladesh over a 20-year period from 1989 to 2009, using LANDSAT satellite images were performed by Sarwar and Woodroffe, 2013. They concluded that, the seaward margin of the Sundarbans in western Bangladesh has retreat rates of up to 20 m/yr. In the Noakhali-Feni coastal zone, rates of erosion were balanced by rapid accretion of the main promontory by more than 600 m/yr. Meghna estuary was especially dynamic with land deposition trend. Rates of change were more subdued in the Chittagong and Cox's Bazaar coastal zones of southeast Bangladesh. The overall area changed relatively little across the entire coastline over the 20-year period with land gain of up to 315 km^2, countered by land loss of about 307 km^2. So there is net overall land gain observed all over in Bangladesh.

However the methods used for shoreline change detection for Bangladesh were based on End Point Rate (EPR) statistics which only considers two shoreline locations: the oldest and the newest. But keeping in mind the dynamicity of the coastal Bangladesh, several temporal images should be used to detect short term changes. Regression techniques were used in the works of Dolan, Fenster and Holme, 1991 and Genz et al., 2007 to determine shoreline change rate where they considered several shorelines of the same area of interest but different years. In this study the shoreline change is determined using both EPR and Linear Regression Rate (LRR) methods. These methods are utilized vitally in shoreline change statistics calculation in the works of Bouchahma and Yan, 2012, Oyedotun, 2014, Kuleli et al., 2011 etc. In this study, Linear Regression Rate has been considered to detect the change statistics of the shoreline geometry of coastal Chittagong and based on the rate a crude prediction for the year 2050 has been made.

2. METHODOLOGY

In order to conduct the study, it was necessary to detect shoreline boundary. First of all, subset of the raw satellite imagery was taken so that it falls within the area of interest (Bouchahma and Yan, 2012). Then the radiometric correction of the image was done to convert the raw Digital Number (DN) to Top of Atmospheric (ToA) Reflectance (Chander, Markham and Helder, 2009) and Mcfeeters Normalized Difference Water Index (NDWI) was calculated from it (Mcfeeters, 1996). After that, Otsu's Binary Thresholding Method was applied to form a binary image which facilitated to segregate water feature from non-water feature (Otsu, 1979). As a result, the coinciding line with the physical interface of water and non-water feature was extracted as shoreline (Boak and Turner, 2005). All of the temporal images were processed using the above method to extract shoreline. After that, cell to cell comparison was made to detect the extent of spatial land area withdrawal and gain (Bouchahma and Yan, 2012). Digital Shoreline Analysis System (DSAS) (an ArcGIS extension) was used to measure change statistics of the shorelines linear regression method (Thieler et al., 2017).

2.1 Study area and data

Chittagong district of Bangladesh is selected as study area to see the shoreline geometry in terms of temporal and spatial change. The shoreline is divided into three segments according to their three different spatial distributions based on the confluence of the Karnafuli and the Shangoo River with the Bay of Bengal, namely, northern segment, in the north part of Karnafuli, middle segment, in the middle of Karnafuli and Shangoo and southern segment situated in the south of Shangoo. They are designated as A, B and C in figure 1. These segments represent 3 sites of Chittagong district namely Chittagong Town, Anowara and Banshkhali respectively.

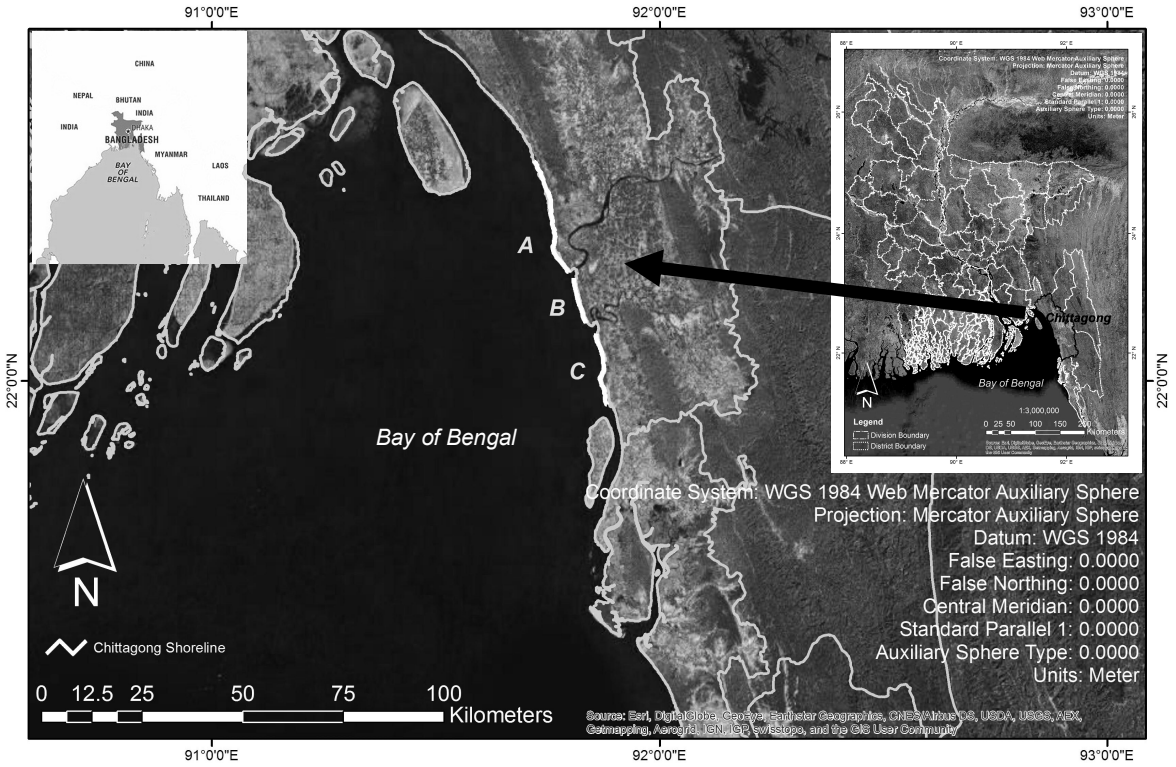

Figure 1: Location of the study area

Multi temporal LANDSAT images were used to monitor shoreline positional change from the year 1977 to 2017. LANDSAT satellite images are generated from the MSS, TM, ETM and OLI sensor platforms which collect different reflected spectral bands of lights from the earth objects (Chander, Markham and Helder, 2009). These LANDSAT images were acquired from the USGS (United States Geological Survey) website (https://earthexplorer.usgs.gov/) which provides NASA (National Aeronautics and Space Administration) archived LANDSAT images (USGS, 2017). The images were selected considering the acquisition date of the data. The dry season of Bangladesh, typically late winter season most likely has less cloud cover (table 1) and for analyzing images sits in a quite favorable condition (Queensland Government, 2007). The properties of the satellite images are given in table 1.

Table 1: Properties of LANDSAT satellite images used in the study

Respective year	Date Acquired (M/D/Y)	Sensor	Path/Row	Land Cloud Cover	Spatial Resolution	Projected Co-ordinate system
1977	01/02/1977	LANDSAT_2 MSS	146/45	0.00	60m	WGS_1984 _46N
1980	01/14/1980	LANDSAT_3 MSS	146/45	0.00	60m	WGS_1984 _46N
1988	02/12/1988	LANDSAT_5 TM	136/45	1.00	30m	WGS_1984 _46N
1993	01/24/1993	LANDSAT_5 TM	136/45	0.00	30m	WGS_1984 _46N
1997	01/19/1997	LANDSAT_5 TM	136/45	0.00	30m	WGS_1984 _46N
2002	02/26/2002	LANDSAT_7 ETM	136/45	0.00	30m	WGS_1984 _46N
2007	02/24/2007	LANDSAT_7 ETM	136/45	0.00	30m	WGS_1984 _46N

Respective year	Date Acquired (M/D/Y)	Sensor	Path/Row	Land Cloud Cover	Spatial Resolution	Projected Co-ordinate system
	01/23/2007*	LANDSAT_7 ETM	136/45	1.00	30m	WGS_1984 _46N
2014	01/02/2014	LANDSAT_8 OLI	136/45	0.07	30m	WGS_1984 _46N
2017	01/02/2017	LANDSAT_8 OLI	136/45	0.01	30m	WGS_1984 _46N

*The Landsat 7 images of the year 2007 have data gaps due to problem with scan line corrector. The data gap was masked using another image of the same acquisition year (Yin et al., 2017). The image denoted by the asterisk is used to fill gaps of the other one.

2.2 Image pre-processing and radiometric correction procedure

The LANDSAT satellite images were provided with pixel values representing digital numbers (DN) which were required radiometric correction for better accuracy and scientific analysis as mentioned by Chander et al., 2009 (figure 2a). Moreover, in order to calculate NDWI, DN has to be converted to ToA reflectance for better performance and is proven in the works of (Alesheikh et al., 2007), (Zhai et al., 2015), (Haque and Basak, 2017), (Gao, 1996) etc. For LANDSAT MSS, TM and ETM sensor derived images, Chander, 2009 suggested to convert DN to Radiance using the following formula:

$$L_\lambda = \left(\frac{LMAX_\lambda - LMIN_\lambda}{Q_{calmax} - Q_{calmin}}\right)(Q_{cal} - Q_{calmin}) + LMIN_\lambda$$

Or,

$$L_\lambda - G_{rescale} \times Q_{cal} + B_{rescale}$$

And Radiance is converted to ToA reflectance using the following formula:

$$\rho_\lambda = \frac{\pi \cdot L_\lambda \cdot d^2}{ESUN_\lambda \cdot \cos\theta_s}$$

For LANDSAT OLI images ToA reflectance can be converted from DN using the following formula directly (U.S. Geological Survey, 2016):

$$\rho_\lambda = \frac{M_p \times Q_{cal} + A_p}{\sin\theta_E}$$

The values of Q_{cal} Q_{calmin} Q_{calmax} $LMIN_\lambda$ $LMAX_\lambda$ θ_E M_p A_p are provided with the LANDSAT image in a metadata file. d, $ESUN_\lambda$ both are calculated using the earth sun distance chart and mean exoatmospheric solar irradiance chart provided by Chander, 2009. All the images used were level 1 data product, so they were already orthorectified, geometrically corrected and co-registered. The formula incorporates sun angle correction too. Figure 2b shows the resulting change of pixel values from conversion of DN to ToA reflectance.

Here,

$$G_{rescale} = \frac{LMAX_\lambda - LMIN_\lambda}{Q_{calmax} - Q_{calmin}}$$

$$B_{rescale} = LMIN_\lambda - \left(\frac{LMAX_\lambda - LMIN_\lambda}{Q_{calmax} - Q_{calmin}}\right) Q_{calmin}$$

Where,

L_λ = Spectral radiance at the sensor's aperture [W / (m^2 sr μm)]

Q_{cal} = Quantized calibrated pixel value [DN]

Q_{calmin} = Minimum quantized calibrated pixel value corresponding to $LMIN_\lambda$ [DN]

Q_{calmax} = Maximum quantized calibrated pixel value corresponding to $LMAX_\lambda$ [DN]

$LMIN_\lambda$ = Spectral at-sensor radiance that is scaled to Q_{calmin} [W / (m^2 sr μm)]

$LMAX_\lambda$ = Spectral at-sensor radiance that is scaled to Q_{calmax} [W / (m^2 sr μm)]

$G_{rescale}$ = Band-specific rescaling gain factor [W / (m^2 sr μm) / DN]

$B_{rescale}$ = Band-specific rescaling bias factor [W / (m^2 sr μm)]

ρ_λ = Planetary ToA reflectance [unitless]

π = Mathematical constant equal to ~3.14159 [unitless]

d = Earth–Sun distance [astronomical units]

$ESUN_\lambda$ = Mean exoatmospheric solar irradiance [W / (m^2 μm)]

θ_s = Solar zenith angle [degrees] *sin will be used for using elevation angle (θ_E)

θ_E = Solar elevation angle [degrees]

M_p = Reflectance multiplicative scaling factor for the band [unitless]

A_p = Reflectance additive scaling factor for the band [unitless]

2.3 Spectral index:

There are many Remote Sensing Based Water Feature Indices to delineate water and non water features such as Normalized Difference Water Index (NDWI) (Mcfeeters, 1996), (Gao, 1996), Normalized Difference Moisture Index (NDMI) (Wilson and Sader, 2002), Modified Normalized Difference Water Index (MNDWI) (Xu and Xulin, 2014), Water Ratio Index (WRI) (Shen and Li, 2010), Normalized Difference Vegetation Index (NDVI) (Rouse et al., 1973), Automated Water Extraction Index (AWEI) (Feyisaa et al., 2014) etc. Because multi-temporal sattelite LANDSAT images were used in this study a suitable index had to be chosen that uses the band common in all historical and current sensors (MSS, TM, ETM, OLI). Though both the Mcfeeters, 1996 NDWI and NDVI index is calculated using Green and Near Infrared band of the sattelite image which are common bands attainable by all LANDSAT sensors (Khorram et al., 2012), the NDWI proposed by (Mcfeeters, 1996) is best for delineating water features with great accuracy (Mcfeeters, 2013) and also the result of Comparison of NDWI Results between Theoretical and Manually Adjusted Threshold proves to be most accurate than other mentioned indices (Das and Pal, 2016). The ToA reflectance of Green and Near Infrared band of the sattelite images were used for calculating Mcfeeters NDWI (Mcfeeters, 1996). It is calculated using the following formula:

$$\mathrm{NDWI} = \frac{\mathrm{Green}_{\mathrm{ToA}} - \mathrm{NIR}_{\mathrm{ToA}}}{\mathrm{Green}_{\mathrm{ToA}} + \mathrm{NIR}_{\mathrm{ToA}}}$$

Here,

$\mathrm{Green}_{\mathrm{ToA}}$ = Top of atmospheric (ToA) reflectance of green band

$\mathrm{NIR}_{\mathrm{ToA}}$ = Top of atmospheric (ToA) reflectance of near infrared band

The NDWI image gives a value ranges from +1 to -1 where typically the positive value represents water and the negative value represents non-water feature as described by Mcfeeters in 1996 (figure 2c).

2.4 Segregation of water and non-water feature:

The NDWI image typically gives positive result for water feature and negative for non-water feature (Mcfeeters, 1996). But it is scene specific and a histogram based thresholding is necessary to create a binary image (0 and 1) depicting water and non water feature (Ji, Zhang, and Wylie, 2009). Binary threshold segmentation method of (Otsu, 1979) was applied on the NDWI images to separate the land from the sea (figure 2d). The threshold calculated automatically to divide the image into two main segment water and land. This segmentation gave improved accuracy for shoreline extraction as the value of the threshold presented by Otsu is set according to the local characteristics (Bouchahma and Yan, 2012). The MSS images had a spatial resolution of 60m (table 1) which were re-sampled to 30m to match with other sensor provided images.

2.5 Post processing of binary raster image

Some isolated pixels that differ from surrounding pixels were generalized by filtering. A 3 × 3 mode filter has been applied for this post-processing operation that replaced the isolated pixels to the most common neighboring class (either water class or non water class) (Ahmed and Ahmed, 2012) (Bartuś, 2014). The jagged boundaries of the water and non water classes were smoothened by using boundary clean tool that eliminates less significant groups of pixels creating small-surfaces (Bartuś, 2014). Raster binary image was then converted to vector and the abutting line of water and non water class was traced to extract final shoreline (figure 2e). Some of the line features were manually manipulated so that it coincides with the actual real time shoreline and this was performed using visual interpretation of RGB raster imagery.

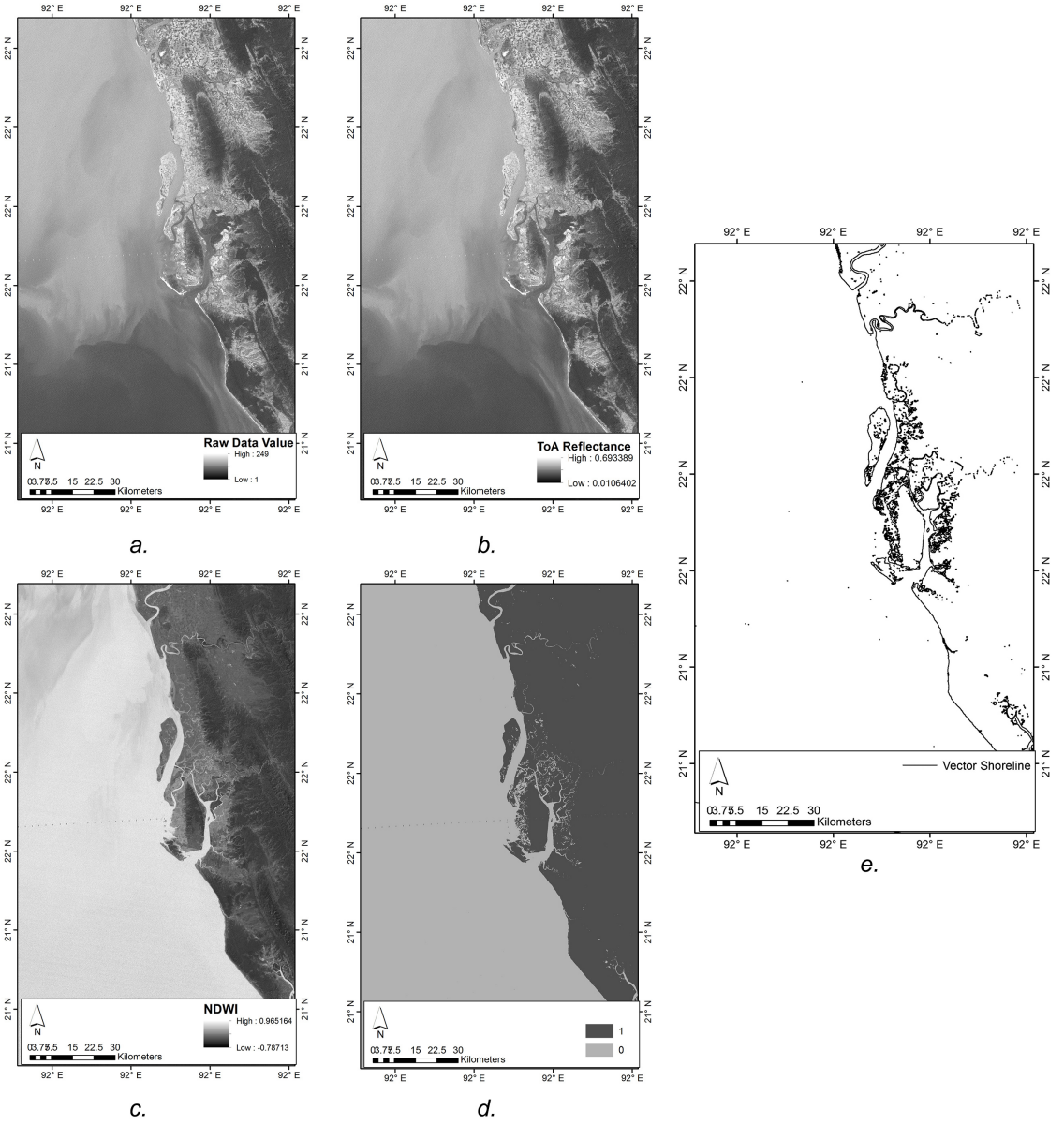

Figure 2: The resulting output from applying the methodological workflow. [a.] The raw LANDSAT satellite image derived from USGS containing DN values; [b.] The corrected image from converting DN to ToA reflectance; [c.] NDWI image derived by applying the Mcfeeteres formula; [d.] Obtained binary image by applying Otsu's Binary Thresholding formula (1=Land and 0=water); [e.] Vector line data representing shoreline

2.6 Statistical parameters used:

Digital Shoreline Analysis System (DSAS) were used to perform change statistics calculation (Thieler et al., 2017) which is capable of calculating Shoreline Change Envelope (SCE) considering 9 points, Net Shoreline Movement (NSM), End Point Rate (EPR) and Linear Regression Rate (LLR). These parameters are widely used in shoreline statistics (Dolan, Fenster and Holme, 1991), (Genz et al., 2007) and DSAS is capable of calculate them automatically. 9 shoreline of the same area for different years were considered. 50m spaced and 1km long transect lines were casted from offshore to landward from a baseline situated 200m Off Coast. +/- 5m uncertainty and 95% confidence interval was set as default parameter to calculate change statistics. DSAS generates transects that are cast

perpendicular to the baseline at a user-specified spacing along-shore (figure 3). The transect shoreline intersections along this baseline are then used to calculate the rate-of-change statistics (Bouchahma and Yan, 2012).

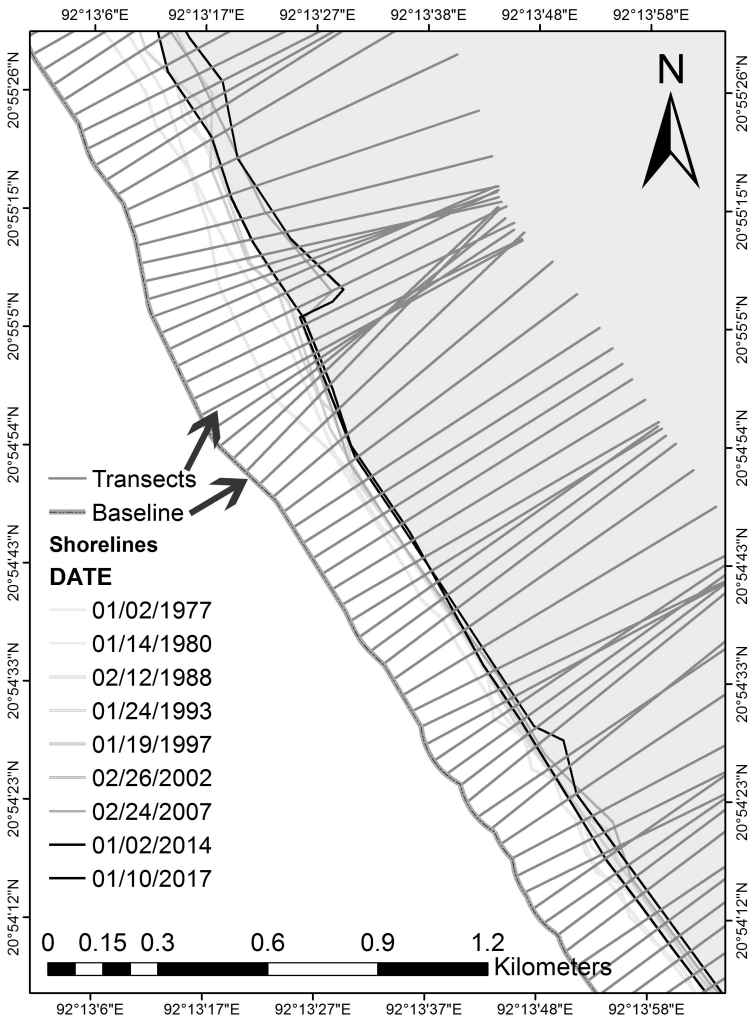

Figure 3: The distances from the baseline to each intersection point along a transect are used to compute EPR and LRR statistics

2.7 Land loss and gain calculation:

The differences of the values of the two binary thresholded images were made using Raster Calculator in ArcGIS to determine the land loss and gain value within the two designated years. It is a simple yet effective change detection method used by (Bouchahma and Yan, 2012) and (Kuleli et al., 2011). For both the images, Water class was reclassified to value 2 and non-water class was reclassified to value 1. The resulting image difference gives values 0, -1 and +1 result. The image differenciation were done using ArcGIS software. From the attribute table, the pixel counts were converted to square kilometers and land withdrawal and land deposition for two different years were computed.

3. RESULTS AND DISCUSSION

The SCE is the distance between the Coastline farthest from and closest to the baseline at each transect between the study time period. It doesn't represent rate. The result shows that in segment A the shoreline has moved farthest in the Beribadh Area near Patenga which is

more than 700 meters (figure 4). Shoeline movement is less significant in segment B and C, although the northern most part of segment C shows some significant movement throughout the study time period.

NSM Reports the distance between the oldest and youngest Coastlines for each transect. It indicates the shifting towards either land or sea. In segment A, Beribadh Area near Patenga has almost 400m landward shifting whereas the same area near norththern Zeley Para shows 600m seaward shifting. Other parts of the B and C segments shows less significant shifting of shoreline (figure 4).

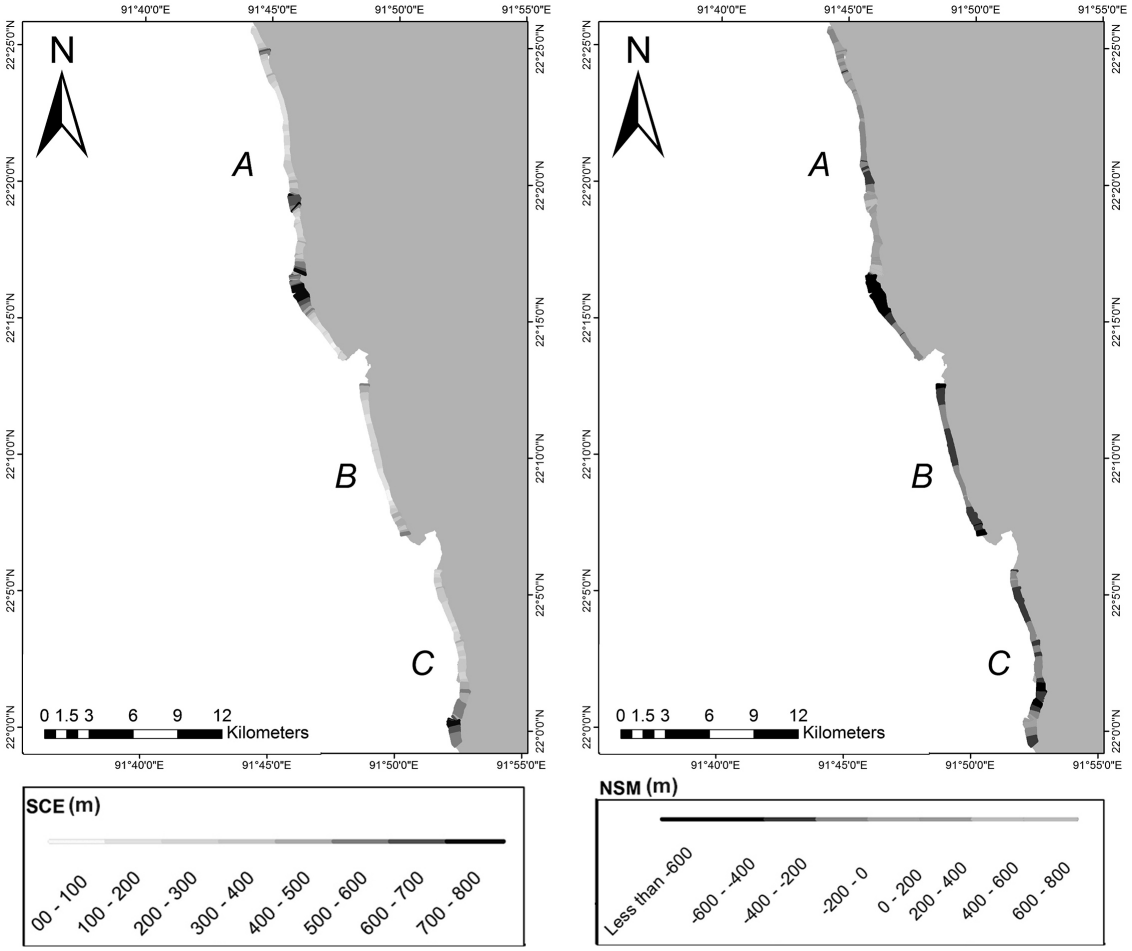

Figure 4: Shoreline Change Envelope (SCE) and Net Shoreline Movement (NSM) (values are in meter)

In this study the rate of change statistics was calculated using LRR method. Additionally EPR was calculated to compare the results. LRR considers all the 9 year's shoreline position whereas EPR considers only the youngest and the oldest (Thieler et al., 2017). As a result, in terms of accuracy, the performance of LRR is superior to EPR. Still, both has been calculated and plotted in graph. Graphically, the results seem quite similar. In segment A, both seaward and landward shifting trend of the shoreline is observed. Seaward shifting rate is high in the Zeley Para Beribadh Area (>16 m/yr) and landward shifting rate is high near Patenga Beach area (>18 m/yr). Segment B shows somewhat low landward shifting rate in Anowara area. Segment C also follows somewhat similar trend in Banshkhali area although in the southern part, some seaward shifting is seen near Maheshkhali. EPR and LRR shows

an average difference of 0.3m (figure 5). Overall in Chittagong, landward shifting of shoreline is significant in all the segments.

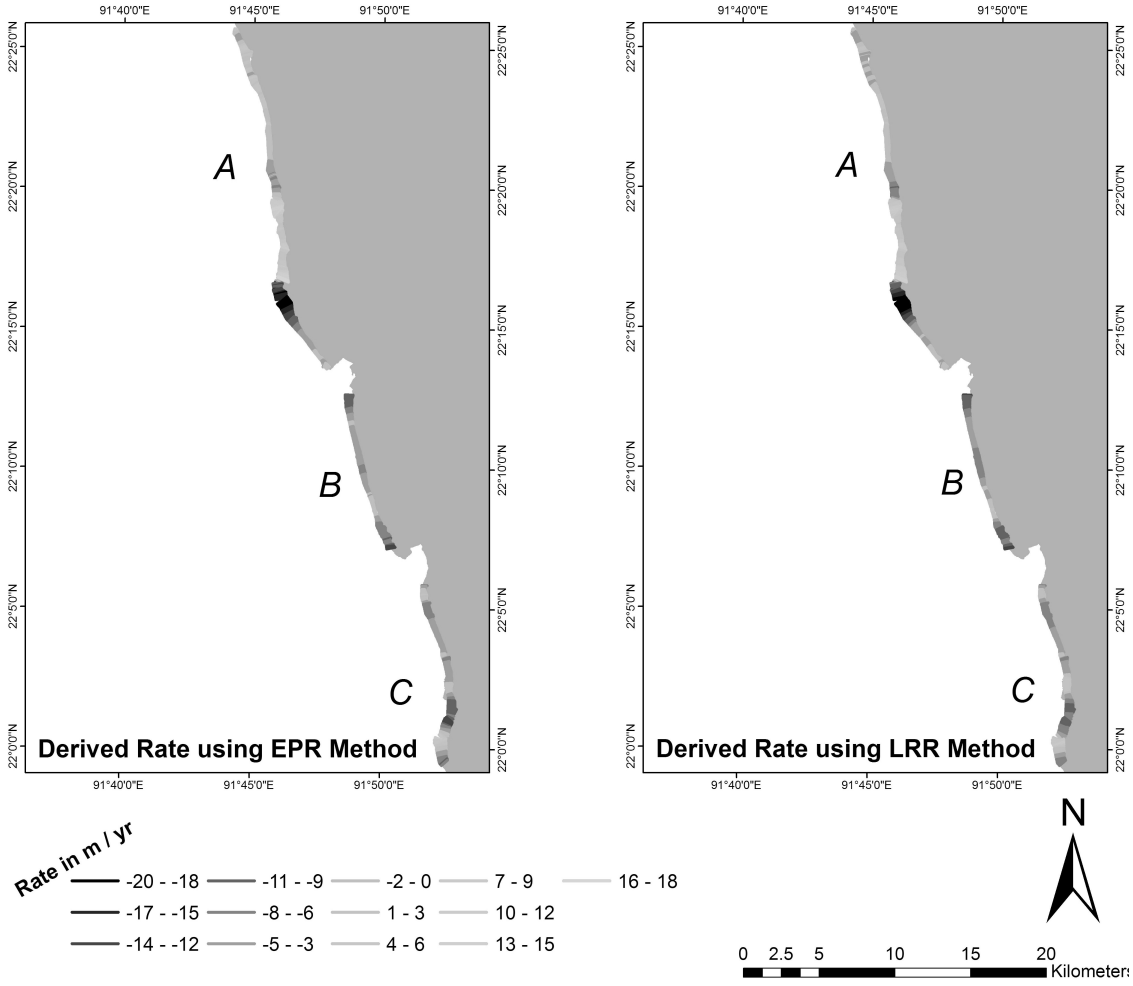

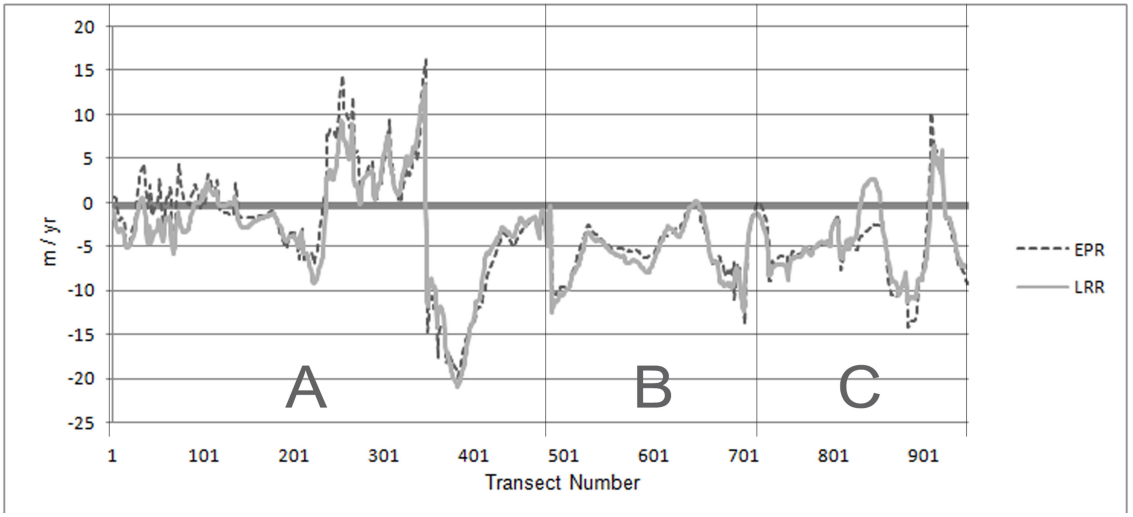

Figure 5: The resulted rates of shoreline changes (land withdrawal or deposition) estimated at each transect are plotted alongshore of the study area

Analysis based on the calculation of land area geometry shows that, the shoreline is shifting towards landward in the entire study area with different rates. In the northern segment, the

average rate is 2.56 m/yr. More than 3.36 km^2 land area was withdrawn and 1.76 km^2 land area was gained. In the middle segment, the rate of shoreline shifting is 6.01 m/yr and more than 2.9 km^2 area was lost. No significant land area is gained. In the southern segment, the average shifting rate of 4.37 m/yr is seen landwards and more than 6.4 km^2 area was lost. Little over 0.17 km^2 land area was gained. Overall, for the last 40 years, a 12.66 km^2 land area withdrawn and 1.93 km^2 land area loss are observed along the shoreline of Chittagong district. The results are summarized in table 2.

Table 2: Change Statistics and Loss-gain results

Segment	EPR Method Average Rate (m / yr)	LRR Method Average Rate (m / yr)	Net Land Area (sq km) loss (1977-2017)	Net Land Area (sq km) gain (1977-2017)	Total
A	-1.7995	-2.557	3.356	1.768	-1.588
B	-5.430	-6.012	2.902	0	-2.902
C	-4.825	-4.371	6.418	0.175	-6.243
Grand Total					**-10.733**

Using the LRR method, the rate derived was also used to depict a crude picture of the shoreline position in the year 2050. The distance from the current shoreline and future shoreline position was used to calculate the predicted land area loss and gain. In segment A, 1.01 km^2 of land area will be gained and 2.43 km^2 of land area will be withdrawn. So, overall, 2.43 km^2 of land area will be lost. No land area will be gained in segment B and 2.5 km^2 of land area will be lost. In segment C, 1.22 km^2 of land area will be deposited and a massive 7.85 km^2 of land area will be extincted (figure 6).

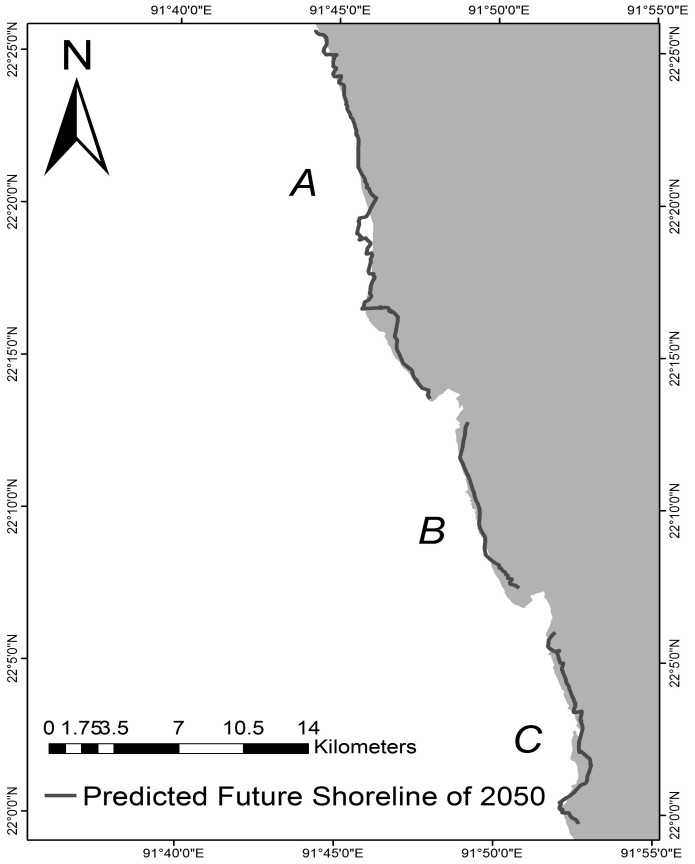

Figure 6: Predicted shoreline for the year 2050

4. CONCLUSION

The historical evolution and temporal morphodynamics of shoreline position and geometry are of significant importance in evaluating the spatial dynamics of the coastal system behaviour (Oyedotun, 2014). The study is aimed towards the development of a method for automatic measurement of shoreline changes of Chittagong coastal region using LANDSAT data and hence indicating the dynamics and trend in change in shoreline geometry. Overall, landloss is more prominent in Chittagong and the trend of landward movement of the coastline in different segments indicates sea level rise is at motion. However, land gain has been remarkable around the area of Beribadh, Zeley Para and also in the south part of Banshkhali area. It is noteworthy that the statement of the extent of sea level rise will submerge Bangladesh's coastal area (Brammer, 2013) is somewhat an exaggerated statement which is proved by the prediction of shoreline for Chittagong. This study points out the areas that need special consideration while making zoning plan or other structure plan. It is also important to keep monitor the changes around the potential land loss prone areas and take in consideration these changes on the future urban and tourism planning.

ACKNOWLEDGEMENTS

This research work was funded by *Directorate of Research and Extension, Chittagong University of Engineering and Technology, Chittagong-4349, Bangladesh*. We express our gratitude to our colleagues from *Chittagong University of Engineering and Technology* who provided intuition and adroitness that tremendously supplemented the research.

REFERENCES

Ahmed, B., and Ahmed, R. (2012). Modeling Urban Land Cover Growth Dynamics Using Multi-Temporal Satellite Images: A Case Study of Dhaka, Bangladesh. *International Journal of Geo-Information , 1*, 3-31.

Alesheikh, A. A., Ghorbanali, A., and Nouri, N. (2007). Coastline change detection using remote sensing. *International Journal of Environmental Science and Technology , 4* (1), 61-66.

Bartuś, T. (2014). Raster images generalization in the context of research on the structure of landscape and geodiversity. *Geology, Geophysics and Environment , 40* (3), 271–284.

Boak, E. H., and Turner, I. L. (2005). Shoreline Definition and Detection: A Review. *Journal of Coastal Research , 21* (4), 688–703.

Bouchahma, M., and Yan, W. (2012). Automatic Measurement of Shoreline Change on Djerba Island of Tunisia. *Computer and Information Science , 5* (5), 17-24.

Brammer, H. (2013). Bangladesh's dynamic coastal regions and sea-level rise. *Climate Risk Management , 1*, 51-62.

Chander, G., Markham, B. L., and Helder, D. L. (2009). Summary of current radiometric calibration coefficients for Landsat MSS, TM, ETM+, and EO-1 ALI sensors. *Remote Sensing of Environment, 113*, 893–903.

Das, R. T., and Pal, S. (2016). IDENTIFICATION OF WATER BODIES FROM MULTISPECTRAL LANDSAT IMAGERIES OF BARIND TRACT OF WEST BENGAL. *International Journal of Innovative Research and Review , 4* (1), 26-37.

Dolan, R., Fenster, M. S., and Holme, S. J. (1991). Temporal analysis of shoreline recession and accretion. *Journal of Coastal Research , 7*, 723-744.

Dolan, R., Hayden, B. P., May, P., and May, S. K. (1980). The reliability of shoreline change measurements from aerial photographs. *Shore and Beach , 48* (4), 22–29.

Erener, A., and Yakar, M. (2012). Monitoring Coastline Change Using Remote Sensing and GIS Technologies. *International Conference on Earth Science and Remote Sensing. 30*, pp. 310-315. Hong Kong: Lecture Notes in Information Technology.

Feyisaa, G. L., Meilbya, H., Fensholtb, R., and Proudb, S. R. (2014). Automated Water Extraction Index: A new technique for surface water mapping using Landsat imagery. *Remote Sensing Environment , 140*, 25-35.

Gao, B. (1996). NDWI A Normalized Difference Water Index for Remote Sensing of Vegetation Liquid Water From Space. *Remote Sensing Environment , 58*, 257-266.

Genz, A. S., Fletcher, C. H., Dunn, R. A., and Frazer, L. (2007). The predictive accuracy of shoreline change rate methods and alongshore beach variation on Maui, Hawaii. *Journal of Coastal Research , 23* (1), 87-105.

Haque, M. I., and Basak, R. (2017). Land cover change detection using GIS and remote sensing techniques: A spatio-temporal study on Tanguar Haor, Sunamganj, Bangladesh. *The Egyptian Journal of Remote Sensing and Space Sciences* , in press.

Ji, L., Zhang, L., and Wylie, B. (2009). Analysis of Dynamic Thresholds for the Normalized Difference Water Index. *Photogrammetric Engineering and Remote Sensing , 75* (11), 1307–1317.

Khorram, S., Koch, F. H., van der Wiele, C. F., and Nelson, S. A. (2012). *Remote Sensing.* New York: Springer.

Kostiuk, M. (2002). USING REMOTE SENSINGDATA TO DETECT SEA LEVEL CHANGE. *Land Satellite Information.*

Kuleli, T., Guneroglu, A., Karsli, F., and Dihkan, M. (2011). Automatic detection of shoreline change on coastal Ramsar wetlands of Turkey. *Ocean Engineering , 38*, 1141–1149.

Li, X., and Damen, M. C. (2010). Coastline change detection with satellite remote sensing for environmenta lmanagement of the Pearl River Estuary, China. *Journal of Marine Systems , 82*, S54–S61.

Mcfeeters, S. K. (1996). The use of normalized difference water index (NDWI) in the delineation of open water features. *International Journal of Remote Sensing , 17* (7), 1425–1432.

Mcfeeters, S. K. (2013). Using the Normalized Difference Water Index (NDWI) within a Geographic Information System to Detect Swimming Pools for Mosquito Abatement: A Practical Approach. *Remote Sensing , 5*, 3544-3561.

Mukhopadhyay, A., Mukherjee, S., Mukherjee, S., Ghosh, S., Hazra, S., and Mitra, D. (2012). Automatic shoreline detection and future prediction: A case study on Puri Coast, Bay of Bengal, India. *European Journal of Remote Sensing , 45*, 201-213.

Otsu, N. (1979). A threshold selection method from gray level histograms. *IEEE Transactions on Systems, Man and Cybernetics , 9* (1), 62-66.

Oyedotun, T. D. (2014). *Geomorphological Techniques.* London: British Society for Geomorphology.

Queensland Government. (2007). *Wetland Mapping and Classification Methodology.* Queensland: Department of Environment and Heritage Protection.

Rouse, J. W., Haas, R. H., Schell, J. A., and Deering, D. W. (1973). Monitoring Vegetation Systems in the Great Plains with ERTS (Earth Resources Technology Satellite). *Third Earth Resources Technology Satellite Symposium* (pp. 309-317). Greenbelt: NASA.

Sarwar, M., and Woodroffe, C. D. (2013). Rates of shoreline change along the coast of Bangladesh. *Journal of Coastal Conservation , 17* (3), 515-526.

Shen, L., and Li, C. (2010). Water Body Extraction from Landsat ETM+ Imagery Using Adaboost. *Proceedings of 18th International Conference on Geoinformatics* (pp. 1-4). Beijing: Geographical Society of China.

Siripong, A. (2010). DETECT THE COASTLINE CHANGES IN THAILAND BY REMOTE SENSING. *International Archives of the Photogrammetry, Remote Sensing and Spatial Information Science , XXXVIII* (8), 992-996.

Thieler, E. R., Himmelstoss, E. A., Zichichi, J. L., and Ergul, A. (2017). *Digital Shoreline Analysis System (DSAS) version 4.0—An ArcGIS extension for calculating shoreline change (ver. 4.4, July 2017).* U.S. Geological Survey Open-File Report 2008-1278.

U.S. Geological Survey. (2016). *LANDSAT 8 (L8) DATA USERS HANDBOOK.* Sioux Falls: EROS.

USGS. (2017, October 25). *About USGS*. Retrieved May 2, 2017, from USGS: https://earthexplorer.usgs.gov

Wilson, E. H., and Sader, S. A. (2002). Detection of forest harvest type using multiple dates of Landsat TM imagery. *Remote Sensing of Environment , 80*, 385–396.

Xu, D., and Xulin, G. (2014). Compare NDVI extracted from Landsat 8 imagery with that from Landsat 7 imagery. *American Journal of Remote Sensing , 2* (2), 10-14.

Yin, G., Mariethoz, G., Sun, Y., and McCabe, M. F. (2017). A comparison of gap-filling approaches for Landsat-7 satellite data. *The International Journal of Remote Sensing , 38* (23), 6653-6679.

Zhai, K., Wu, X., Qin, Y., and Du, P. (2015). Comparison of surface water extraction performances of different classic water indices using OLI and TM imageries in different situations. *Geo-spatial Information Science , 18* (1), 32-42.